Available online at www.sciencedirect.com

SCIENCE DIRECT®

Earth and Planetary Science Letters 236 (2005) 135–147

EPSL

www.elsevier.com/locate/epsl

Flow banding in obsidian: A record of evolving textural heterogeneity during magma deformation

Helge M. Gonnermann*, Michael Manga[1]

Department of Earth and Planetary Science, University of California, 307 McCone Hall, Berkeley, CA 94720-4767, USA

Received 29 October 2004; received in revised form 11 April 2005; accepted 12 April 2005
Available online 20 June 2005
Editor: S. King

Abstract

We perform a quantitative textural analysis of banding in obsidian from Big Glass Mountain (BGM), Medicine Lake Volcano, California and from Mayor Island (MI), New Zealand. The samples are compositionally homogeneous, with banding defined by variable microlite content (BGM) or vesicularity (MI). The spatial distribution of alternating light and dark bands has a 1/wavenumber power-spectral density, as well as multifractal characteristics. Through the use of simple mathematical models, we demonstrate that formation of the observed banding structure is consistent with a continuous deformational reworking of magma. Our results indicate that changes in crystallinity (vesicularity) were concurrent with magma deformation and are random multiples of the total amount of crystallinity (vesicularity) that was already present at any given time. Banded obsidian from BGM and MI can be found in close spatial proximity to brittle deformational textures. We therefore propose that a key element of banding formation in our samples may be magma brecciation or fragmentation. Fragmentation can result in variable rates of degassing of fragments, which in turn can lead to nonuniform crystal (vesicle) nucleation and growth rates. Repeated fragmentation, welding and subsequent viscous deformation can thus lead to banding formation.

PACS: 91.40.−k; 91.50.Hw; 91.60.Ba; 83.50.−v; 83.70.Hq; 83.80.Nb; 47.20.Ft; 47.50+d; 47.52.+j; 47.53.+n; 47.54.+r; 47.55.−t; 47.70−n
Keywords: volcanology; mixing; flow banding; obsidian; fragmentation; fractal

1. Introduction

Banding in obsidian samples from Big Glass Mountain (BGM), Medicine Lake Volcano, California and from Mayor Island (MI), New Zealand preserves a record of deformation associated with magma ascent, eruption, and emplacement. Alternating light and dark bands ranging in width from tens of microns to

* Corresponding author. Department of Earth and Planetary Sciences, Harvard University, 20 Oxford Street, Cambridge, MA 02138, USA. Tel.: +1 617 496 6796; fax: +1 617 495 8839.
E-mail addresses: gonnermann@eps.harvard.edu (H.M. Gonnermann), manga@seismo.berkeley.edu (M. Manga).
[1] Tel.: +1 510 643 8532; fax: +1 510 643 9980.

0012-821X/$ - see front matter © 2005 Elsevier B.V. All rights reserved.
doi:10.1016/j.epsl.2005.04.031

decimeters are defined by differences in crystallinity (BGM) or vesicularity (MI). Proposed processes for banding formation include viscous magma mixing (e.g., [1–4]), repeated autobrecciation and welding of fragments during flow at the surface (e.g., [5,6]), welding and rheomorphism of pyroclastic fragments (e.g., [7–11]), vapor-precipitated crystallization in stretched vesicles [12], or brittle deformation and welding of fragments during magma ascent in the volcanic conduit [13–16].

Although textural heterogeneity caused by mixing of preexisting parent magmas has received considerable attention, the origin of compositionally homogeneous banded lavas, such as BGM or MI samples, remains relatively unexplored. This is an important area of study because crystal or bubble nucleation and growth are intimately linked to magma degassing [17–19], which in turn is responsible for the buildup of overpressure required for the transition from effusive to explosive eruptive behavior [20–25]. One important unanswered question is whether the deformational process that results in banding is separate from (i.e., subsequent to) the actual development of textural heterogeneity or if both processes are related in some manner.

2. Approach

The main goal of our analysis is to assess whether banding in the BGM and MI obsidian samples preserves a record from which we can gain insight into the general nature of the underlying formational process, and hence about magma ascent and emplacement processes inaccessible to direct observation. We use spectral and multifractal analyses of banding to test if the formation of textural heterogeneity occurred prior to deformation, or if both processes are concurrent. We focus on obsidian because the optical transparency allows measurements of structures to be made over a broad range of scales. Moreover, the obsidian samples under consideration bear evidence of a genetic relation between brittle magma deformation and banding formation. A petrographic description of both samples is provided in Section 3.

In Section 4 we describe the results from powerspectral and multifractal analyses of each sample. Powerspectral analysis permits the identification of a scale-invariant record, whereas multifractal analysis allows the identification of a multiplicative formational process. In the context of the two samples analyzed here, this corresponds to a repeated (continuous) change in crystallinity (BGM) or vesicularity (MI) that is a small random multiple of the total amount already present. Such a process is called multiplicative and, in contrast to cumulative processes, results in binomial frequency distribution of the given attribute. Using a series of hypothesis tests (Section 5), we provide constraints on the required dynamics of such a process. Finally, in Section 6 we discuss brittle deformation of magma as a possible physical mechanism for the formation of banding in BGM and MI obsidian samples.

3. Samples

Banding in BGM and MI obsidian is defined by alternating planar layers of varying color as a consequence of varying micorocrystallinity (BGM) or microvesicularity (MI). In cross-section this layering ranges in thickness from microns to decimeters and may attain lengths of up to several meters. Often, the layering can be distorted or folded [26].

3.1. BGM obsidian

BGM is a 900-year-old rhyolite-to-dacite obsidian flow [27–30]. It is the youngest part of the Medicine

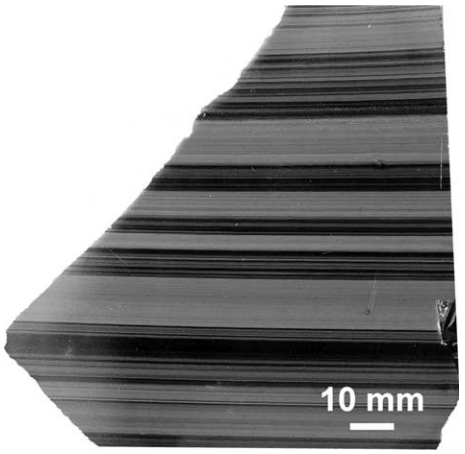

Fig. 1. Photograph of banded obsidian sample from Big Glass Mountain, Medicine Lake Volcano, California.

Fig. 2. Two different views of the same sample of obsidian from Big Glass Mountain. The sample is a rectangular slab and (a) is the side view perpendicular to (b). The sample shows a continuous gradation from angular, fused fragments (right third), to deformed fragments (middle), to well-developed banding (left third), consistent with brittle deformation, welding of fragments and subsequent viscous deformation.

Lake composite shield volcano [27] and provides an example of the effusive emplacement of a cubic kilometer-sized volume of silicic melt. Effusion was preceded by an explosive phase that resulted in the deposition of tephra over an area of approximately 320 km^2 [31]. BGM therefore provides an excellent example of a sizable silicic eruption with a transition from explosive to effusive behavior. The youngest eruptive sequence includes obsidian that is ubiquitously banded (Fig. 1), with some samples bearing evidence for a genetic relation between fragmentation and banding (Fig. 2).

Banding is predominantly defined by varying concentrations of pyroxene microlites (Fig. 3), with a higher microlite content resulting in a darker color. At times, dark bands also contain increased concentrations of oxides (e.g., the darkest band in Fig. 3). However, overall there appears to be no compositional difference or difference in water content (J. Castro, personal communication) between individual bands of BGM obsidian. Some samples show a continuous gradation from angular, fused fragments (right third of Fig. 2), to deformed fragments (middle of Fig. 2), to well-developed banding (left third of Fig. 2), indicating that brittle deformation, welding of fragments and subsequent deformation may have resulted in at least some of the observed banding.

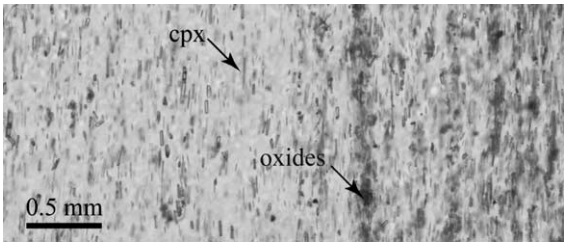

Fig. 3. Photomicrograph of obsidian from Big Glass Mountain. Banding is generally defined by varying microlite content in a glassy matrix. Some dark bands also contain oxides.

3.2. MI obsidian

MI is the visible portion of a 700-m-high and 15-km-wide Quaternary shield volcano [32]. Despite its uniform peralkaline magma composition, MI's history includes virtually the full range of known eruption styles over a wide range of eruption sizes [33,34], including fire-fountaining and spatter-fed lava flows, such as the 8-ka obsidian flow from which our sample was collected [7,10,34]. Banding in the MI obsidian sample under consideration is predominantly defined

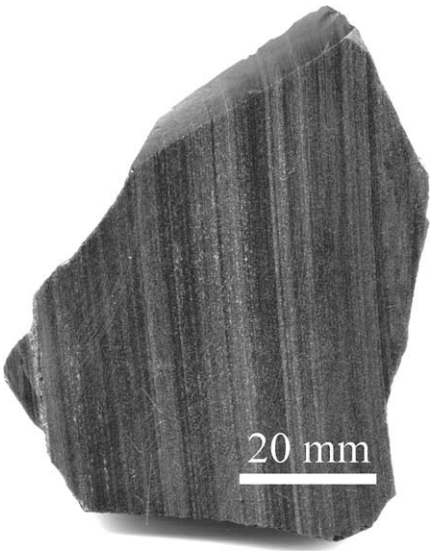

Fig. 4. Polished sample of Mayor Island banded obsidian (provided by K. V. Cashman, University of Oregon).

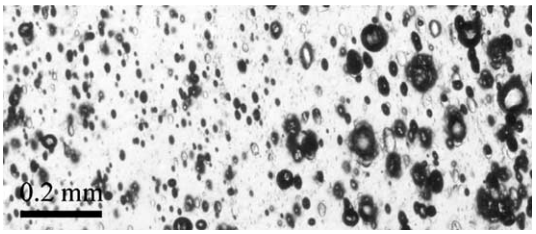

Fig. 5. Photomicrograph of obsidian from Mayor Island. Banding is defined by varying vesicularity.

by varying bubble content (Figs. 4 and 5), with higher vesicularity corresponding to lighter bands. The MI sample provides a sample of banded obsidian with evidence of a clastogenic origin and close spatial association with magma brecciation [7].

3.3. Digitized banding

Our subsequent analysis is based on photomicrographs of polished obsidian samples. Because of the degree of magnification, each analyzed sample image actually represents a composite of a number of high-resolution digital photographs. The digitized sample from BGM has a length of 200 mm and a resolution of 2 μm/pixel (Fig. 6a). Equivalently, we obtain a digital record with 5 μm/pixel resolution from a 55-mm-long sample of MI obsidian, provided by K. V. Cashman, University of Oregon (Fig. 6b). The cumulative frequency distribution of resultant gray-scale color index values, $0 \le C_i \le 1$, from each sample is shown in Fig. 7. Consistent with the terminology used in multifractal analysis, each digitized sample will hereafter be referred to as the "record."

We normalize gray-scale color index, C_i, for each pixel, i, as

$$\phi_i = [C_i - \min(C)]\left[\sum_{i=1}^{N} C_i - N\min(C)\right]^{-1} \quad \text{where} \quad \sum_{i=1}^{N} \phi_i = 1. \tag{1}$$

Here ϕ_i is the normalized gray-scale color index, hereafter also referred to as the "measure." It is not our goal to draw detailed quantitative estimates of process parameters from our analysis. Instead we only seek to establish if BGM and MI samples are multifractal or not. Unlike for example Perugini et al. [4], where bands are defined by compositional variations, we do not obtain a precise calibration of color index to microcrystallinity or microvesicularity of our samples. It should be noted that, our transformation from natural samples to measures does not bias the outcome of our analysis, as will be shown in Section 5.

4. Analysis of banding

4.1. Power spectrum

The wavenumber power spectrum, $S(k)$, is one of the most often used tools for studying complex spatial patterns, because of its compact quantitative description of the presence of many spatial scales [35]. We use the multitaper method (e.g., [36] and references therein) as a spectral estimator, where data windows are given by discrete prolate spheroidal sequences [37] that effectively minimize spectral leakage. This technique is well suited for detailed spectra with a large dynamic range. We tested different taper sequences to minimize leakage effects or other artifacts and find that an estimator with NW=4 (time bandwidth for the Slepian sequences) is well suited for our analysis. Both BGM and MI spectra (Fig. 8) are characterized by a $1/\text{wavenumber}$ scaling of spectral power, $S(k) \sim k^{-1}$, indicating scale invariance.

4.2. Multifractal analysis

Monofractal records are often characterized by k^{-1} power spectra. They have the same scaling properties throughout the entire signal and can be characterized by a single fractal dimension. Records produced by multiplicative processes, in contrast, are usually found to be multifractal [38,39]. Instead of being characterized by a single fractal dimension, they have locally varying scaling properties that contain valuable information regarding the formational process (e.g., [39]). For example, the energy-cascading process embodied by fluid turbulence generates a multifractal time series of velocity fluctuations that is mathematically well represented by a multiplicative model [39]. We therefore use a multi-

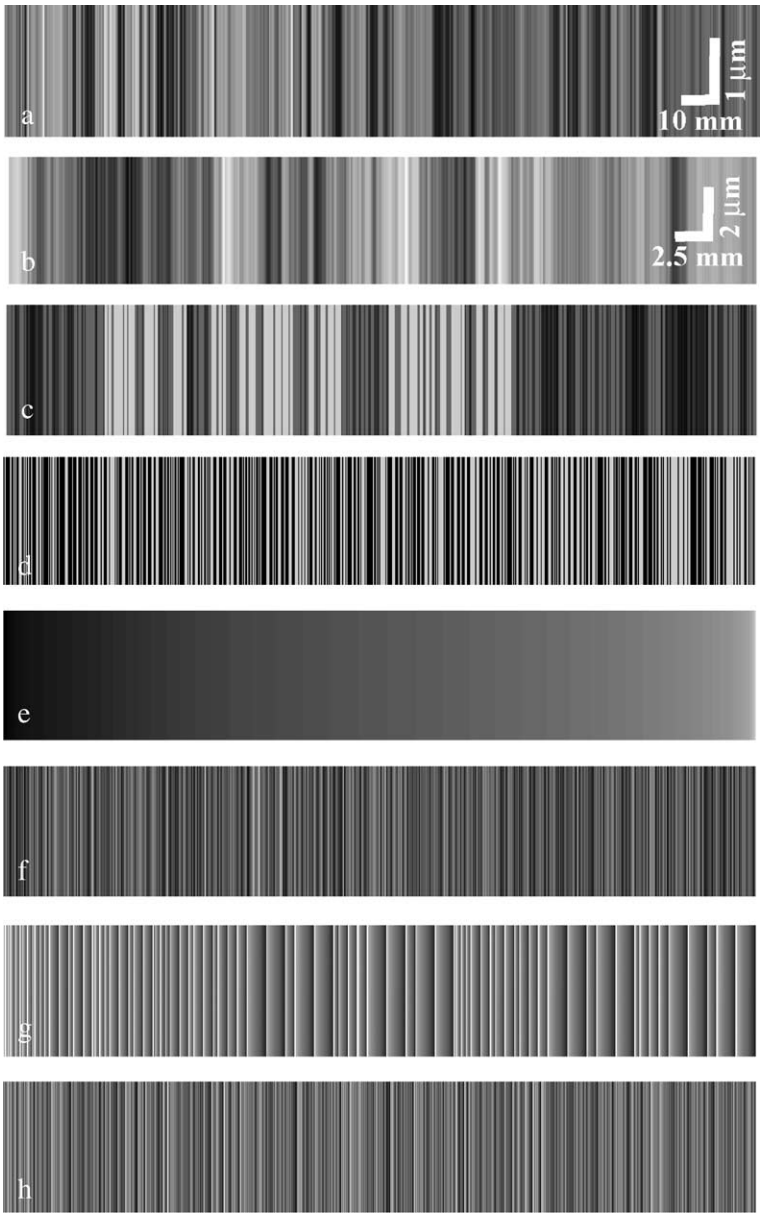

Fig. 6. Banding for (a) Big Glass Mountain (BGM) (200 mm length), (b) Mayor Island (55 mm length), (c) Multiplicative cascade (MC) based on the two-scale cantor set, (d) MC with alternating black and white bands only, (e) BGM pixels sorted by color index, (f) BGM with random redistribution of pixels, (g) Baker's map of the sorted BGM from panel (e) after four iterations, (h) Baker's map of sorted BGM from panel (e) after six iterations.

fractal analysis to test whether banding in BGM and MI obsidian is multifractal and, hence, possibly preserves a record of a multiplicative formational process.

4.2.1. Method

Multifractal records can be characterized by the singularity spectrum, $f(\alpha)$, of some measure, $\phi(x)$, which in our case represents the normalized color

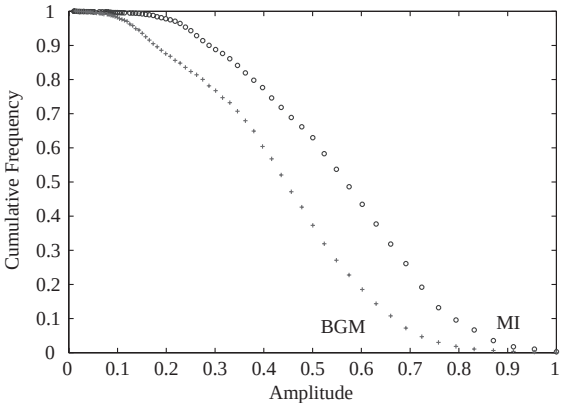

Fig. 7. Cumulative frequency distribution of the measure (normalized gray-scale color index) for Big Glass Mountain and Mayor Island obsidian samples.

index as a proxy for microcrystallinity (BGM) or vesicularity (MI). It is possible to evaluate the presence of different scaling laws throughout the record via the integrated measure

$$\mu_i = \int_{i-L/2}^{i+L/2} \phi \mathrm{d}x, \text{ where } \sum_{i=1}^{N} \mu_i = 1. \quad (2)$$

Here L is the length of a record segment centered at position i, with the entirerecord of length X subdivided into $N=X/L$ segments. The $f(\alpha)$ singularity-spectrum provides a mathematical description of the spatial distribution of ϕ over the entire record, with the singularity strength, α, defined by

$$\mu_i(L) \sim L_i^{\alpha}. \quad (3)$$

Counting the number of segments, $N(\alpha)$, where $\mu_i(L)$ has a singularity strength, α, allows the loose definition of $f(\alpha)$ as the fractal (Hausdorff) dimension of the part of the record with singularity strength of α [38,40]

$$N(\alpha) \sim L^{-f(\alpha)}. \quad (4)$$

For a given segmentation length, or an equivalent box-counting dimension, L, the value of α will vary with position i. As a consequence, $f(\alpha)$ characterizes the spatial complexity of the actual record. If the record is uniformly fractal (monofractal) or not fractal at all, then there will be only one value of α, reducing $f(\alpha)$ to a single point. If the record is complexly (though not randomly) structured so that its fractal dimension changes with position, then there exists a range of α with different Hausdorff dimensions, $f(\alpha)$. The more complexly structured the record is, the broader the spectrum will be.

The spectrum $f(\alpha)$ can be obtained by considering different moments, μ_i^q, of the integrated measure. Here the parameter ϕ provides a "microscope" for exploring different regions of the banding structure. As ϕ is varied, different subsets of the record, which are associated with different scaling exponents, α, become dominant. The singularity spectrum can then be obtained from [40]

$$f(q) = \lim_{L\to 0} \frac{\sum_i \mu_i^q(L)\ \log[\mu_i^q(q,L)]}{\log L} \quad (5)$$

and

$$\alpha(q) = \lim_{L\to 0} \frac{\sum_i \mu_i^q(L)\ \log[\mu_i(L)]}{\log L}. \quad (6)$$

In practice, the slopes of $\sum_i \mu_i^q(L)\ \log[\mu_i^q(q,L)]$ and $\sum_i \mu_i^q(L)\ \log[\mu_i(L)]$ versus $\log L$ are estimated to obtain $f(\alpha)$ and α, respectively. In multifractal analysis there are a number of potential problems that must avoided ([41] and references therein). Most importantly, care must be taken to only consider the range of $\log L$ over which these graphs do actually represent

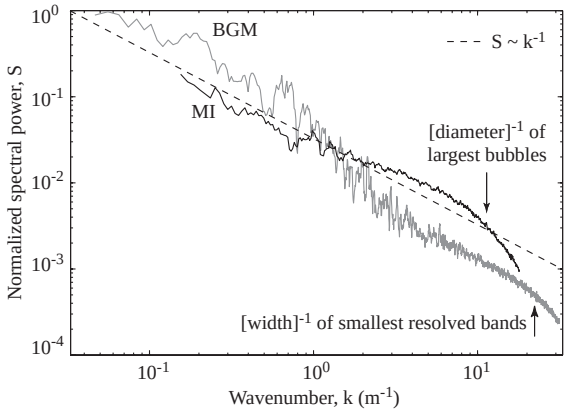

Fig. 8. Power spectra for Big Glass Mountain and Mayor Island obtained from averaging the spectra from 200 rasters of the digital photomicrograph of each obsidian sample. Both spectra are characterized by a 1/wavenumber scaling of spectral power ($S(k)\sim k^{-1}$) indicating scale invariance.

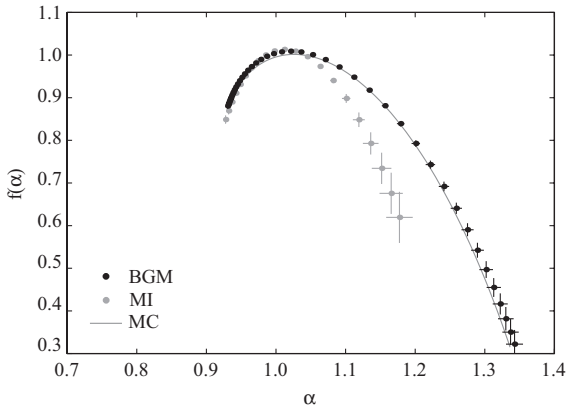

Fig. 9. Singularity spectra obtain by the Chhabra–Jensen method [40]. $f(\alpha)$ for Big Glass Mountain (BGM) and Mayor Island (MI) are broad, indicating a multifractal record. The error of estimation is evaluated from the variance in the estimation of the slope (Section 4.2.1). Also shown is the multifractal singularity spectrum for the multiplicative cascade generated via the two-scale Cantor set [38]. Both BGM and MI singularity spectra are consistent with a multiplicative process.

linear trends. If they do not represent linear trends, then the record is not truly multifractal, but could still result in a singularity spectrum with multifractal character. Therefore, $f(q)$ and $\alpha(q)$ were estimated for max $(\delta_{\mathrm{BGM}}, \delta_{\mathrm{MI}}) \leq L \leq \min(X_{\mathrm{BGM}}, X_{\mathrm{MI}})/10$. Here δ_{BGM} represents the width of the smallest resolved band of the BGM sample, δ_{MI} is the average diameter of the largest bubbles of the MI sample, X_{BGM} is the length of the BGM sample, and X_{MI} is the length of the MI sample. These ranges correspond to linear segments of the aforementioned graphs and are identical for both samples, so that there is no bias in the analysis. Furthermore, it should be noted that we compared our results for the entire BGM sample (200 mm in length) with analyses of segments of the BGM sample with lengths identical to that of the MI sample (55 mm). In all cases, the BGM singularity spectrum essentially has the multifractal characteristics shown in Fig. 9. Finally, we compared results from the Chhabra–Jensen method with the Legendre-transform method [38] and found the results shown here to be robust.

4.2.2. Results

The singularity spectrum (Fig. 9) indicates that banding structure of BGM and MI obsidian are multifractal, implying that banding may have formed

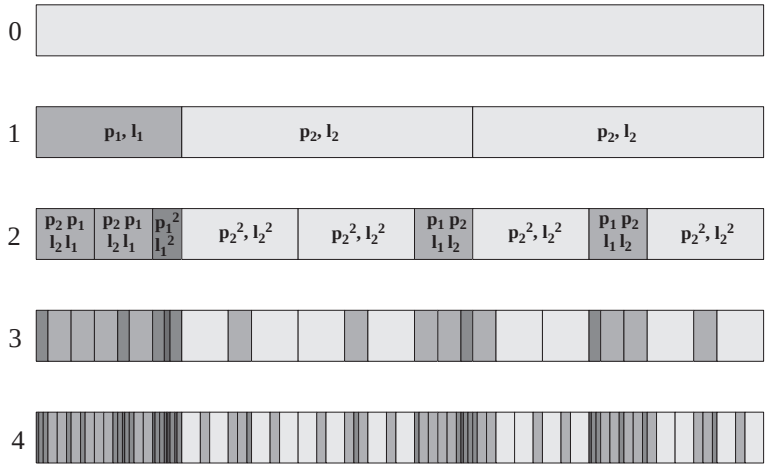

Fig. 10. Multifractal record generated by a multiplicative cascade (after four iterations) based on the two-scale Cantor set [38]. The segment of unit length and uniform measure (denoted by gray-scale color) shown at step 0 is cut into three segments, one of length l_1 and two of length l_2. The measure of the first segment is multiplied by a factor of p_1, and that of the two other segments is multiplied by a factor of p_2, where $p_1 > p_2$. Each of the resulting three segments shown at step 1 are, in turn, cut into three segments, one of length $l_1 l_{\mathrm{seg}}$ and two of length $l_2 l_{\mathrm{seg}}$. Here l_{seg} denotes the length of the given segment shown at step 1. The resultant segment lengths are either l_1 l_2, l_1^2, or l_2^2. Concurrently, the measure of each segment from step 1 is again multiplied by either p_1 if its length is $l_1 l_{\mathrm{seg}}$, or by p_2 otherwise. The resultant segments and measures, denoted by different shades of gray (p_1 p_2, p_1^2, or p_2^2), are shown at step 2. The process is then repeated for steps 3 and 4. It should be noted that the spatial sequence into which each segment is subdivided is chosen randomly at any given step.

Table 1
Comparison of obsidian samples

Record	MF[a]	$(S\sim k^{-1})$[b]	MP[c]	Implications
Big Glass Mountain (BGM)	Y	Y	Y	Concurrent microlite growth and deformation into bands
Mayor Island (MI)	Y	Y	Y	Concurrent formation of variable vesicularity and deformation
Cantor (MC)	Y	Y	Y	Concurrent development of heterogeneity and deformation
Cantor binary	N	N	N	No binomial measure
BGM randomized	N	N	N	Decoupled microlite growth and deformation into bands
Baker's map	Y	N	N	Decoupled microlite growth and deformation into bands

Cantor map with hypothesis tests.
[a] Multifractal.
[b] S is spectral power and k is wavenumber.
[c] Multiplicative process.

through a multiplicative processes. To illustrate that this is feasible, we show $f(\alpha)$ for a multifractal record produced by a simple mathematical model representative of a multiplicative processes (Fig. 9). It is based on the two-scale Cantor set (MC) [38], where a unit interval is randomly subdivided into three segments: two of given length l_2, and one of length l_1 (Fig. 10). The two former intervals each receive a proportion, p_2, of the total measure, and the latter interval receives a proportion given by p_1, as indicated by the different color shading. This process is recursively repeated for each segment from the previous iteration (Fig. 10). In an idealized sense this could, for example, be equivalent to a fragmentation process with a given scaling for fragment sizes (l_1 and l_2) and an embedded enrichment or depletion (p_1 and p_2) of some measure (e.g., volatile content, crystal or vesicle content, chemical or isotopic component). This idealized multiplicative process with $l_1=p_1=1/5$ and $l_1+2l_2=p_1+2p_2=1$ results in the banding shown in Fig. 6c and provides an excellent match to the BGM singularity spectrum (Fig. 9). It is important to note, that this implies that microcrystallinity (vesicularity) evolved concurrently to and integral with magma deformation in BGM (MI) obsidian.

5. Alternative hypotheses

To assess the limitations of our results, we test several alternative hypotheses, summarized in Table 1.

5.1. Black and white banding

Fig. 6d shows the banding structure generated by the same multiplicative process as shown in Fig. 10, but with banding defined by only two alternating values of the measure ϕ (black or white). In contrast to the BGM and MI samples, as well as the MC model, this binary banding is not multifractal, and its singularity spectrum consists of a single point, shown in Fig. 11. As already discussed by Turcotte [42], this demonstrates the importance of a binomial measure produced through a multiplicative enrichment or fractionation process in the generation of a multifractal record (e.g., [43–45]).

5.2. Randomized BGM

Fig. 6e shows the banding of the BGM sample (Fig. 6a), but sorted from darkest to lightest normalized color index, ϕ. For our second test, we randomly redistributed this measure. This hypothesis is motivated by the possibility that microlite content or

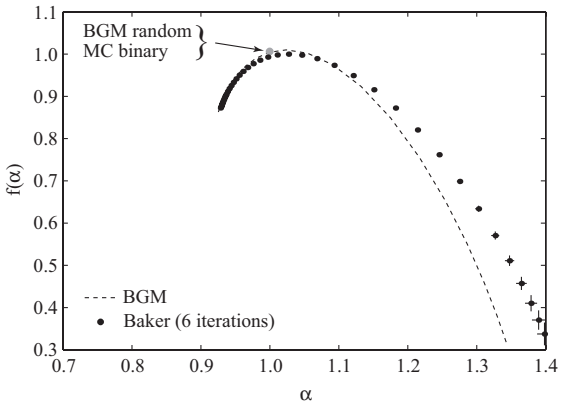

Fig. 11. Singularity spectra for the different hypothesis tests. Big Glass Mountain with randomized pixels (Fig. 6f) and the multiplicative cascade with only black-and-white bands (Fig. 6d) are monofractal and plot as single points. The spectrum for the generalized Baker's map after six iterations (Fig. 6g) is multifractal and similar to that of the Big Glass Mountain sample (Fig. 6a), shown as the dashed line.

vesicularity may vary, for example, radially or vertically before the actual mixing process, as suggested by Castro and Mercer [46]. In this case the "mixing" process is of a purely random nature (as opposed to chaotic or otherwise). The resultant record (Fig. 6f) is not multifractal (Fig. 11). We can conclude that a binomial measure alone does not suffice for a multifractal record, implying that a random formational process, or random "mixing" of a preexisting measure, is not sufficient for the formation of multifractal banding.

5.3. Chaotic mixing via Baker's map

In our third test, we examine the possibility that a preexisting measure (e.g., microlite content) of identical probability distribution as the BGM sample (Fig. 6e) could be redistributed through a chaotic mixing process to result in banding with similar characteristics as the BGM sample. Similar to Section 5.2, this hypothesis is motivated by the possibility of a preexisting gradation in microlite content or vesicularity prior the actual mixing process [46].

A simple mathematical model that has been used to represent the characteristics of chaotic mixing is the generalized Baker's map (e.g., [35,47,48]). We performed calculations using several different parameterizations of the generalized Baker's map. Although details varied between different versions, the overall results were the same. We therefore only show results for one version of this map. This version has a ratio of segmentation lengths identical to that of the multiplicative Cantor process (Fig. 10). The Baker's map spatially redistributes a given measure on a unit square and is mathematically equivalent to the process of stretching and folding in chaotic fluid mixing, illustrated in Fig. 12. Mathematically, the process is given by the mapping

$$\begin{matrix} x_{n+1} \\ y_{n+1} \end{matrix} = \begin{cases} l_2^* x_n, y_n / l_2^* & \text{if } y_n < l_2^* \\ l_2^* + l_1^* x_n, \left(y_n - l_2^*\right)/l_1^* & \text{if } l_2^* < y_n \le l_2^* + l_1^* \\ l_2^* + l_1^* + l_1^* x_n, \ \left(y_n - l_2^* - l_1^*\right)/l_1^* & \text{if } l_2^* + l_1^* < y_n. \end{cases} \tag{7}$$

Here $l_1^* = l_1 + \theta$, $l_2^* = (1 - l_1^*)/2$, and θ is a number chosen randomly at each iteration, with $\theta \le l_1/2 \le \theta$. The Baker's map is analogous to closed-system chaotic mixing, in which the original measure is conserved throughout (i.e., for all iterations $\sum_{i=1}^{N} \phi_i = 1$). With respect to BGM (MI), the Baker's map implies that microlite (vesicle) growth and banding formation are decoupled. The singularity spectrum (Fig. 9) obtained from this map is multifractal and is very similar to the BGM sample (Fig. 11). However, the power spectrum allows a clear distinction. Whereas power spectra of BGM, MI (Fig. 8), and the MC model are characterized by $S \sim k^{-1}$, the power spectrum for the Baker's map with initial measure derived from the BGM sample has $S \sim k^{-\beta}$, with $\beta \approx 1.5 - 2$. This result indicates, consistent with results from mixing studies (e.g., [4,47,48]), that a magma with preexisting nonuniform microlite content, or vesicularity, can be mixed, resulting in banding with multifractal properties. However, the power spectrum is not likely to have the $S \sim k^{-1}$ scaling observed in BGM and MI samples.

5.4. Summary

The results of the hypothesis tests, summarized in Table 1, demonstrate (1) that banding has to be defined by binomial frequency distribution of textural heterogeneity (Section 5.1); and (2) that spatial redis-

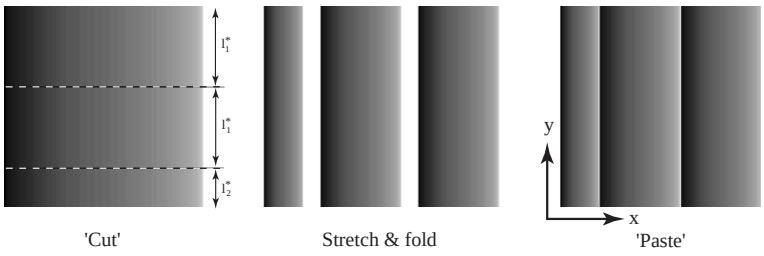

Fig. 12. Schematic representation of the modified Baker's map (e.g., [47,48]), where the initial measure is based on the sorted Big Glass Mountain of Fig. 6e. This map represents a chaotic redistribution of a preexisting measure.

tribution of preexisting heterogeneity is insufficient to reproduce banding characteristics of BGM and MI samples (Sections 5.2 and 5.3). The latter also shows that using normalized gray-scale color index will not bias our results in terms of the multifractal vs. monofractal character of banding.

6. Application

We have shown that a multiplicative process, whereby the development of textural heterogeneity and the spatial redistribution thereof are concurrent and interrelated, is consistent with banding of obsidian samples from BGM and MI. The multiplicative cascade represented by the two-scale Cantor set (Fig. 10) embodies the multiplicative nature of an idealized physical process, but is not indicative of the mechanics of such a process. In this section we propose a hypothetical physical process that is multiplicative and consistent with the formation of banded obsidian. It consists of repeated cycles of brittle magma deformation followed by welding of fragments and subsequent viscous deformation into bands. A schematic illustration of this process is shown in Fig. 13.

6.1. Brittle deformation

Brittle deformation of magma occurs when strain rates locally exceed the ability of the melt to deform viscously [49–51], causing it to break into fragments like a brittle solid. This transition is referred to as the glass transition (e.g., [49–52]). Variable degassing of magma fragments may result in variable crystallization (vesiculation) kinetics [17–19,53] over relatively short distances. For example, microlite content, which defines banding in BGM obsidian samples, varies by less than a few volume percent [54], suggesting that realistic conditions (i.e., length and time scales) for the development of observable textural heterogeneity are not difficult to achieve.

Because of the displacement and rotational component associated with simple shear deformation, fragments from different spatial locations could easily become juxtaposed. Once strain rates have relaxed magma fragments can become welded and deformed viscously. Viscous deformation of texturally heterogeneous, welded fragments will then result in banding. This process may occur repeatedly (continuously) during ascent or surface emplacement of magma. It is, except for welding of fragments and viscous deformation, essentially equivalent to the comminution of rocks in fault or shear zones, where banding may also be observed [55].

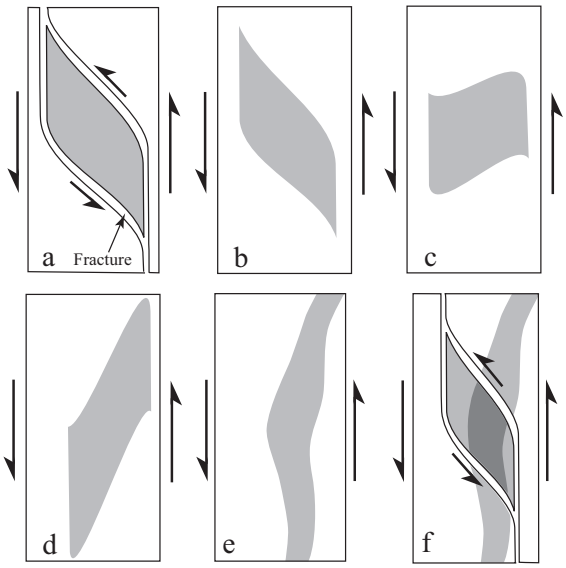

Fig. 13. Idealized schematic illustration of our conceptual model for banding formation via brittle deformation of magma. (a) Brittle deformation during simple shear. The single fragment shown here undergoes a change in texture (e.g., microlite content or vesicularity), indicated by the darker color. Note the presence of fractures and the sigmoidal geometry, which is similar to tension gashes. Tension gashes often form in en echelon arrays. They may be precursors to shear localization (e.g., [61] and references therein) and can be rotated by deformation either during or after formation. (b) The fragments have welded into one coherent piece. (c–e) Viscous deformation under simple shear into a band. (f) A second episode of fragmentation and multiplicative change in texture indicated by the change in color. Note that the band which formed during the previous cycle is broken into several pieces and becomes "reworked". Repetition of this process will result in a broad range of textural heterogeneity and in an increasingly finer banding structure. The two-scale Cantor's map (Fig. 10) is a simple one-dimensional representation of this process.

Banding has been observed in close association with brittle deformation in BGM samples (Fig. 2), as well as at Mayor Island [7,10] and elsewhere (e.g., [5,6]). In addition, banding has also been observed within dissected conduits [15,56], indicating that, at least in some cases, banding may form during magma ascent in the conduit. Recent work suggests that shear strain rates during the ascent of silicic

magmas can exceed the glass transition [14,15,57], even for effusive eruptions that produce lava flows and domes. We therefore surmise that banding formation may occur both during ascent of silicic magmas and during surface emplacement.

6.2. Viscous deformation

Castro and Mercer [46] find that differences in the degree of volatile loss can account for some variability in microlite content in obsidian. However, they ultimately conclude that varying microlite content is more likely to record different ascent rates and residence histories in the volcanic conduit, rather than variations in magma degassing. They suggest that slower magma ascent rates near the conduit walls permit the development of higher crystallinity compared to that of faster ascending magma further in from the conduit walls. Similarly, it has been suggested that varying vesicularity may be caused by variable ascent rates [58], or by a spatially variable temperature distribution [59].

Pervasive banding formation over the observed spatial scales requires repeated stretching and folding, in which nearby parcels of magma can diverge strongly from each other. Unlike brittle deformation, the required divergent stretching is not easily achieved in a highly viscous magma without considerable complexity of the flow geometry (e.g., [60] and references therein). However, complexity of the flow during surface emplacment or in the upper parts of conduits may be more easily achieved than during ascent at depth within the volcanic conduit.

7. Conclusion

We conclude that the observed banding structure in BGM and MI obsidian is consistent with a repeated (or continuous) change in crystallinity or vesicularity that is a small random multiple of the amount already present. Moreover, this textural evolution was concurrent with, or integral to, the mechanical deformation of magma. Such a process creates increasingly finer scales of banding through a cascade to shorter and shorter wavelengths until some cutoff value, given by vesicle or crystal size, is reached [35]. We propose repeated cycles of magma brecciation, welding and subsequent viscous deformation as a feasible mechanism for banding formation. This conceptual model is consistent with the concurrent development of textural heterogeneity through variable crystallization (vesiculation) kinetics as a consequence of variable degassing rates of magma fragments.

Acknowledgments

We thank J.V. Smith, D.W. Dingwell, and two anonymous reviewers for comments and suggestions that helped improve this manuscript. We also thank A. Rust, A.M. Jellinek, and A. Namiki for comments on an earlier version of the manuscript; K.V. Cashman for providing the Mayor Island sample; and T. Teague and M. Calaleta for sample preparation. This work was supported by a National Science Foundation grant and the Garniss Curtis fund to M.M.; and by the Turner Fellowship to H.M.G.

References

[1] S.J. Seaman, Multi-stage magma mixing and mingling and the origin of flow banding in the Aliso Lava Dome, Tumacacori Mountains, southern Arizona, J. Geophys. Res. 100 (1995) 8381–8398.
[2] A. Toramaru, E. Takazawa, T. Morishita, K. Matsukage, Model of layering formation in a mantle peridotite (Horoman, Hokkaido, Japan), Earth Planet. Sci. Lett. 185 (2001) 299–313.
[3] D. Perugini, G. Poli, R. Mazzuoli, Chaotic advection, fractals and diffusion during mixing of magmas: evidence from lava flows, J. Volcanol. Geotherm. Res. 124 (3–4) (2003) 255–279.
[4] D. Perugini, G. Ventura, M. Petrelli, G. Poli, Kinematic significance of morphological structures generated by mixing of magmas: a case study from Salina Island (southern Italy), Earth Planet. Sci. Lett. 222 (2004) 1051–1066.
[5] J.V. Smith, Ductile–brittle transition structures in the basal shear zone of a rhyolite lava flow, eastern Australia, J. Volcanol. Geotherm. Res. 72 (1996) 217–223.
[6] J.V. Smith, Structural analysis of flow-related textures in lavas, Earth-Sci. Rev. 57 (2002) 279–297.
[7] R.J. Stevenson, R.M. Briggs, A.P.W. Hodder, Emplacement history of a low-viscosity, fountain-fed panterlleritic lava flow, J. Volcanol. Geotherm. Res. 57 (1993) 39–56.
[8] G. Kobberger, H.U. Schmincke, Deposition of rheomorphic ignimbrite D (Morgán Formation), Gran Canariz, Canary Islands, Spain, Bull. Volcanol. 60 (1999) 465–485.
[9] J. Gottsmann, D.B. Dingwell, Cooling dynamics of spatter-fed phonolite obisidian flows on Tenerife, Canary Islands, J. Volcanol. Geotherm. Res. 105 (2001) 323–342.

[10] J. Gottsmann, D.B. Dingwell, The thermal history of a spatter-fed lava flow: the 8-ka pantellerite flow of Mayor Island, New Zealand, Bull. Volcanol. 64 (2002) 410–422.
[11] C. Soriano, S. Zafrilla, J. Martí, S. Bryan, R. Cas, G. Ablay, Welding and rheomorphism of phonolitic fallout deposits from the Las Cañadas caldera, Tenerife, Canary Islands, Geol. Soc. Am. Bull. 114 (2002) 883–895.
[12] B.P. Hausback, An extensive, hot, vapor-charged rhyodacite flow, Baja California, Mexico, in: J.H. Fink (Ed.), The Emplacement of Silicic Domes and Lava Flows, Geol. Soc. Am. Spec. Pap., vol. 212, Boulder, Colorado, 1987, pp. 111–118.
[13] G.H. Curtis, Mode of origin of pyroclastic debris in the Mehrten Formation of the Sierra Nevada, Univ. Calif. Publ. Bull. Dep. Geol. Sci. 29 (1954) 453–502.
[14] H.M. Gonnermann, M. Manga, Explosive volcanism may not be an inevitable consequence of magma fragmentation, Nature 426 (2003) 432–435.
[15] H. Tuffen, D.B. Dingwell, H. Pinkerton, Repeated fracture and healing of silicic magma generate flow banding and earthquakes? Geology 31 (2003) 1089–1092.
[16] A.C. Rust, K.V. Cashman, P.J. Wallace, Magma degassing buffered by vapor flow through brecciated conduit margins, Geology 32 (2004) 349–352.
[17] S.E. Swanson, M.T. Naney, H.R. Westrich, J.C. Eichelberger, Crystallization history of Obsidian Dome, Inyo Domes, California, Bull. Volcanol. 51 (1989) 161–176.
[18] C. Geschwind, M.J. Rutherford, Crystallization of microlites during magma ascent: the fluid mechanics of recent eruptions at Mount St. Helens, Bull. Volcanol. 57 (1995) 356–370.
[19] J.E. Hammer, K.V. Cashman, R.P. Hoblitt, S. Newman, Degassing and microlite crystallization in pre-climactic events of the 1991 eruption of Mt. Pinatubo, Philipines, Bull. Volcanol. 60 (1999) 355–380.
[20] J.C. Eichelberger, C.R. Carrigan, H.R. Westrich, R.H. Price, Non-explosive silicic volcanism, Nature 323 (1986) 598–602.
[21] C. Jaupart, C.J. Allegre, Gas content, eruption rate and instabilities of eruption regime in silicic volcanoes, Earth Planet. Sci. Lett. 102 (1991) 413–429.
[22] D.B. Dingwell, Volcanic dilemma: flow or blow? Science 273 (1995) 1054–1055.
[23] R.S.J. Sparks, Causes and consequences of pressurization in lava dome eruptions, Earth Planet. Sci. Lett. 150 (1997) 177–189.
[24] C. Jaupart, Gas loss from magmas through conduit walls during eruption, in: J. Gilbert, R. Sparks (Eds.), The Physics of Explosive Volcanic Eruptions, vol. 145, Special Publications, Geological Society, London, 1998, pp. 73–90.
[25] B. Villemant, G. Boudon, Transition from dome-forming to Plinian eruptive styles controlled by H_2O and Cl degassing, Nature 392 (1998) 65–69.
[26] A.C. Rust, M. Manga, K.V. Cashman, Determining flow type, shear rate and shear stress in magmas from bubble shapes and orientations, J. Volcanol. Geotherm. Res. 122 (2003) 111–132.
[27] C.A. Anderson, Volcanoes of the Medicine Lake Volcano, California, Univ. Calif. Publ. Bull. Dep. Geol. Sci. 25 (1941) 347–422.
[28] J.M. Donnelly-Nolan, A magmatic model of Medicine Lake Volcano, California, J. Geophys. Res. 93 (1988) 4412–4420.
[29] J.M. Donnelly-Nolan, D.E. Champion, C.D. Miller, T.L. Grove, D.A. Trimble, Post-11,000-year volcanism at Medicine Lake Volcano, Cacscade Range, Northern California, J. Geophys. Res. 95 (1990) 19693–19704.
[30] T.L. Grove, J.M. Donnelly-Nolan, T. Housh, Magmatic processes that generated the rhyolite of Glass Mountain, Medicine Lake Volcano, N. California, Contrib. Mineral. Petrol. 127 (1997) 205–223.
[31] G. Heiken, Plinian-type eruptions in the Medicine Lake Highland, California, and the nature of the underlying magma, J. Volcanol. Geotherm. Res. 4 (1978) 375–402.
[32] B.F. Houghton, C.J.N. Wilson, Explosive rhyolitic volcanism: the case studies of Mayor Island and Taupo Volcanoes, N. Z., Geol. Surv. Rec., Tasman. 12 (1986) 33–100.
[33] M.D. Buck, R.M. Briggs, C.S. Nelson, Pyrolcastic deposits and volcanic history of Mayor Island, New Zealand, J. Geol. Geophys. 24 (4) (1981) 449–467.
[34] B.F. Houghton, S.D. Weaver, C.J.N. Wilson, M.A. Lanphere, Evolution of a Quaternary peralkaline volcano: Mayor Island, New Zealand, J. Volcanol. Geotherm. Res. 51 (1992) 217–236.
[35] A. Namenson, T.M.J. Antonsen, E. Ott, Power law wavenumber spectra of fractal particle distributions advected by flowing fluids, Phys. Fluids 8 (9) (1996) 2426–2434.
[36] E.J. McCoy, A.T. Walden, D.B. Percival, Multitaper spectral estimation of power law processes, IEEE Trans. Signal Process. 46 (1998) 655–668.
[37] D. Slepian, Prolate spheroidal wave functions. Fourier analysis and uncertainty: V. The discrete case, Bell Syst. Tech. J. 57 (1978) 1371–1978.
[38] T.C. Halsey, M.H. Jensen, L.P. Kadanoff, I. Procaccia, B.I. Shraiman, Fractal measures and their singularities: the characterization of strange sets, Phys. Rev., A 33 (1986) 1141–1151.
[39] C. Meneveau, K.R. Sreenivasan, Simple multifractal cascade model for fully developed turbulence, Phys. Rev. Lett. 59 (1987) 1424–1427.
[40] A. Chhabra, R.V. Jensen, Direct determination of the $f(\alpha)$ singularity spectrum, Phys. Rev. Lett. 62 (1989) 1327–1330.
[41] D. Veneziano, G.E. Moglen, R.L. Bras, Multifractal analysis: pitfalls of standard procedures and alternatives, Phys. Rev., E Stat. Phys. Plasmas Fluids Relat. Interdiscip. Topics 52 (1995) 1387–1398.
[42] D.L. Turcotte, Fractals and Chaos in Geology and Geophysics, Cambridge University Press, Cambridge, UK, 1997.
[43] H.J. De Wijs, Statistics of ore distribution: Part I. Frequency distribution of assay values, Geol. Mijnbouw 13 (1951) 365–375.
[44] H.J. De Wijs, Statistics of ore distribution: Part II. Theory of binomial distribution applied to sampling and engineering problems, Geol. Mijnbouw 15 (1953) 12–24.
[45] C.J. Allègre, Quantitative models of trace element behaviour, Earth Planet. Sci. Lett. 38 (1978) 1–25.
[46] J. Castro, C. Mercer, Microlite textures and volatile contents of obsidians from the Inyo volcanic chain, California, Geophys. Res. Lett. 31 (2004), doi:10.1029/2004GL020489.

[47] J.M. Finn, E. Ott, Chaotic flows and fast magnetic dynamos, Phys. Fluids 31 (1988) 2992–3011.
[48] E. Ott, T.M.J. Antonsen, Fractal measures of passively convected vector fields and scalar gradients in chaotic fluid flows, Phys. Rev., A 39 (7) (1989) 3660–3671.
[49] D.B. Dingwell, S.L. Webb, Relaxation in silicate melts, Eur. J. Mineral. 2 (1990) 427–449.
[50] S.L. Webb, D.B. Dingwell, The onset of non-Newtonian rheology of silicate melts— a fiber elongation study, Phys. Chem. Miner. 17 (1990) 125–132.
[51] D.B. Dingwell, S.L. Webb, Structural relaxation in silicate melts and non-Newtonian melt rheology in geologic processes, Phys. Chem. Miner. 16 (1989) 508–516.
[52] S.L. Webb, D.B. Dingwell, Viscoelasticity, Rev. Mineral. Geochem. 32 (1995) 95–119.
[53] J.E. Hammer, M.J. Rutherford, An experimental study of the kinetics of decompression-induced crystallization in silicic melt, J. Geophys. Res. 107 (2002), doi:10.1029/2001JB000291.
[54] M. Manga, Orientation distribution of microlites in obsidian, J. Volcanol. Geotherm. Res. 86 (1998) 107–115.
[55] K. Otsuki, N. Monzawa, T. Nagase, Fluidization and melting of fault gouge during seismic slip: identification in the Nojima fault zone and implications for focal earthquake mechanisms, J. Geophys. Res. 108 (2003), doi:10.1029/2001JB001711.
[56] M.C. Stasiuk, J. Barclay, M.R. Carroll, C. Jaupart, J.C. Ratté, R.S.J. Sparks, S.R. Tait, Degassing during magma ascent in the Mule Creek vent (USA), Bull. Volcanol. 58 (1996) 117–130.
[57] A. Goto, A new model for volcanic earthquake at Unzen Volcano: melt rupture model, Gephys. Res. Lett. 26 (1999) 2541–2544.
[58] A. Toramaru, Vesiculation process and bubble size distribution in ascending magmas with constant velocities, J. Geophys. Res. 94 (1989) 17523–17542.
[59] A. Toramaru, A. Ishiwatari, M. Matsuzawa, N. Nakamura, S. Arai, Vesicle layering in solidified intrusive magma bodies: a newly recognized type of igneous structure, Bull. Volcanol. 58 (1996) 393–400.
[60] G.A. Voth, G. Haller, J.B. Gollub, Experimental measurements of stretching fields in fluid mixing, Phys. Rev. Lett. 88 (2002), doi:10.1103/PhysRevLett.88.254501.
[61] R.C. Fletcher, D.D. Pollard, Can we understand structural and tectonic processes and their products without appeal to a complete mechanics? J. Struct. Geol. 21 (1999) 1071–1088.